First-principles string molecular dynamics: An efficient approach for finding chemical reaction pathways

Y. Kanai, A. Tilocca, A. Selloni, and R. Car

Citation: The Journal of Chemical Physics **121**, 3359 (2004); doi: 10.1063/1.1773159
View online: https://doi.org/10.1063/1.1773159
View Table of Contents: http://aip.scitation.org/toc/jcp/121/8
Published by the American Institute of Physics

ARTICLES

First-principles string molecular dynamics: An efficient approach for finding chemical reaction pathways

Y. Kanai, A. Tilocca, and A. Selloni
Department of Chemistry, Princeton University, Princeton, New Jersey 08544

R. Car
Department of Chemistry, Princeton University, Princeton, New Jersey 08544 and Princeton Institute for the Science and Technology of Materials (PRISM), Princeton, New Jersey 08544

(Received 9 April 2004; accepted 24 May 2004)

A recently proposed approach, called ''string method,'' allows us to find minimum energy pathways connecting two metastable states of a system [W. E *et al.*, Phys. Rev. B **66**, 052301 (2002)]. So far this approach has been only used with empirical force field parametrizations of the atomic potential energy surface or in the context of macroscopic continuum models. Here we show that the string method can be efficiently combined with first-principles molecular dynamics to provide an accurate description of chemical reaction pathways and barriers. We illustrate the first-principles string molecular dynamics by applying it to the study of a surface chemical reaction, for which extensive experimental and theoretical works are available, namely, the adsorption of H_2 on the reconstructed Si(100) surface. [DOI: 10.1063/1.1773159]

I. INTRODUCTION

The development of computational methodologies for predicting chemical reaction rates from first-principles electronic structure calculations is the focus of a vast amount of current research. This is motivated by the crucial role that chemical reactions play in a variety of processes of interest to chemistry, materials science, and biophysics. Modeling chemical reactions from first-principles microscopic theory is a very challenging goal in several respects. First, a good description of events in which chemical bonds break and form requires accurate electronic structure methodologies. Second, reaction pathways result from the interplay of electronic structure and atomic motions. This requires efficient techniques to determine how changes of atomic configuration affect the electronic bonding structure. Finally, in order to sample reaction pathways one needs algorithms capable of dealing with the rare event nature of most chemical reactions, which are activated processes and occur infrequently on the time scale of molecular dynamics.[1]

First-principles molecular dynamics[2] (FPMD) provides a convenient framework to deal with the first two challenges. In this approach the atomic potential energy surface (PES) is derived ''on the fly'' from the quantum mechanical ground state of the electrons within density functional theory (DFT). DFT calculations are feasible for relatively complex systems containing up to several hundred atoms, yet they are sufficiently accurate to predict correctly the chemical bonding structure and trends in a large class of systems. Using FPMD methodologies one can efficiently relax atomic structures and perform molecular dynamics simulations based on a PES of DFT quality. FPMD simulations, in which the electrons follow adiabatically the atomic motion, are well suited to deal with adiabatic chemical reactions. FPMD, however, does not address the challenge associated with the time scale of chemical reactions. Typically, time scales of few tens of picoseconds are accessible in FPMD simulations. These are many orders of magnitude smaller than the inverse reaction rates of most chemical reactions.

The general issue of rare events has been examined in several recent papers.[1,3–5] In the present context, however, we restrict our attention to reactive processes that are dominated by potential energy rather than entropy changes, and which are well described in terms of one or few minimum energy paths (MEP). A MEP is a path of minimum local energy that connects reactant and product states in configuration space. A MEP defines a scalar reaction coordinate. Once this has been identified, it is straightforward to locate accurately critical points (minima and maxima) along it. A local maximum on the MEP is a saddle point on the PES: It provides the transition state (TS) for the reactive flux between two adjacent minima on a pathway. A rate can be associated to a MEP by means of transition state theory (TST).[6] This is an approximate, but often sufficiently accurate, approach to compute chemical reaction rates. Still, locating a MEP and/or TS on the PES is highly nontrivial, in view of the complexity of the PES. For instance, schemes that search for a TS based on the knowledge of the reactant state and of the local Hessian,[7] apart from requiring computationally expensive second derivatives of the PES, often fail to locate the TS even in case of reactions that are only moderately complex.[3] Robust schemes to locate a MEP are based on the concept of ''chain of states.'' These approaches require knowledge of both the reactant and the product states and represent a transition path by a chain of system replicas describing intermediate states between the reactant and the

product. All the replicas are relaxed simultaneously to find a MEP. A very popular scheme in this class is the nudged elastic band (NEB) method, which has been used extensively in the context of plane-wave DFT calculations,[3,8] particularly for surface problems.[9–11]

The NEB method uses a penalty function to keep the replicas equally spaced on a chain. More recently, a new chain of states approach, called the string method, has been proposed.[4] The string method replaces the penalty function of the NEB method with an exact mathematical constraint that is imposed by Lagrange multipliers. The constraint is associated to a parametrization of the string, which is kept fixed while the string is deformed to find a MEP. Within the string and the NEB methods, the search for a MEP becomes a local optimization problem. This can be solved by suitable dynamics in string space. So far steepest-descent dynamics has been used for this purpose in most implementations. While the NEB has been used extensively in the context of plane-wave DFT calculations, the string method has been used to date only in the context of empirically parametrized force fields.

In this paper we show that the string method can be efficiently combined with FPMD. In FPMD the equations of motion for atomic dynamics are coupled to constrained dynamical equations for the electronic degrees of freedom. In first-principles string molecular dynamics (FPSMD), the equations of motion for the atoms are replaced by a constrained dynamical equation for the string, which is coupled to preconditioned constrained dynamical equations[12] for the electronic degrees of freedom along the string. This has some similarity to the scheme used to combine path integrals with FPMD.[13] In the present context we are interested only in local minimization dynamics, which can be conveniently formulated in terms of damped (second-order) molecular dynamics equations. These equations extend directly to the string case, a technique currently used within Car–Parrinello schemes to simultaneously relax atomic and electronic degrees of freedom. As shown in Ref. 12 this approach is significantly more efficient than steepest-descent dynamics. The constraint on the string parametrization can be incorporated exactly within the numerical accuracy of the adopted dynamical integrators, using a procedure analogous to SHAKE.[14] This extends to the string case, the approach used in Car–Parrinello dynamics to impose the orthogonality constraint on the Kohn–Sham orbitals. The resulting approach is as efficient as the damped FPMD approach is for local optimization. The numerical cost of finding a MEP is therefore roughly equivalent to the cost of a single local structural optimization by damped FPMD times the number of replicas used to represent a string.

We illustrate FPSMD with a realistic application, a surface reaction concerning H_2 adsorption on a Si(100) crystalline surface. Our approach is able to locate efficiently the MEP and the corresponding TS. Our results compare well with previous calculations done on this system using alternative approaches.

The paper is organized as follows: In Sec. II, we present the FPSMD approach, starting from the basic concepts of the string method. In Sec. III, we illustrate our implementation of FPSMD with a realistic numerical application. The final section of the paper (Sec. IV) is devoted to conclusions. Numerical details of the implementation are given in the Appendixes.

II. THEORETICAL APPROACH

A. String method

We consider a multiatomic system whose PES $V(R_1,R_2,\ldots,R_N)$ as a function of the atomic coordinates is known. We indicate by $R\equiv(R_1,R_2,\ldots,R_N)$ a generic configuration of the system. The string method at zero temperature, on which we focus here, is a powerful approach to find transition states when the PES is smooth on the thermal energy scale and its critical points are isolated.[4] Under these circumstances the TS are the saddle points along the MEP that connect two metastable states A and B, which correspond to local minima on the PES. As a consequence, finding the TS requires finding the MEP. In what follows we will indicate by φ a path in configuration space that connects A and B. A MEP φ^* is a path that satisfies

$$(\nabla V[\varphi^*])^{\perp}=0. \tag{1}$$

Here $(\nabla V)^{\perp}$ is the component of $\nabla V \equiv\{\partial V/\partial R_1,\partial V/\partial R_2,\ldots,\partial V/\partial R_N\}$ orthogonal to φ^*. The string method allows us to find φ^*, using an appropriate dynamics in path space.

A finite path, or string, can be given a parametric representation in terms of a scalar variable α defined along the path

$$\varphi=\varphi(\alpha). \tag{2}$$

For instance, α can be the normalized arc length along the path; in this case $0\leqslant\alpha\leqslant 1$ and the two end states A and B correspond to $\alpha=0$ and $\alpha=1$, respectively. This is the choice of parametrization that we adopt in this paper, but other choices are also possible, as discussed in Ref. 4. The parameter α labels a configuration R^{α}, i.e., $\varphi(\alpha)\equiv R^{\alpha}$. The requirement that the parametrization is preserved when a string deforms can be expressed by the constraint

$$\frac{d}{d\alpha}|\varphi_{\alpha}|=0. \tag{3}$$

Here $\varphi_{\alpha}\equiv d\varphi/d\alpha$ and $|\varphi_{\alpha}|=(\varphi_{\alpha}\cdot\varphi_{\alpha})^{1/2}$. Equation (3) states that the local arc length is constant along a string. The constraint in Eq. (3) is equivalent to

$$\varphi_{\alpha}\cdot\varphi_{\alpha}=c, \tag{4}$$

where c is a constant (independent of α). Equation (4) implies that the allowed deformations of a string are those in which the local elastic stretching energy (proportional to $|\varphi_{\alpha}|^2$) is distributed uniformly along the string. Integrating both sides of Eq. (4) between $\alpha=0$ and $\alpha=1$ one obtains

$$\int_0^1|\varphi_{\alpha}|^2 d\alpha=c. \tag{5}$$

By adopting the parametrization in Eq. (2) with the constraint (3) or (4), the condition (1) becomes

$$\{\nabla V[\varphi^*(\alpha)]\}^{\perp} - \lambda(\alpha)\hat{\tau}^*(\alpha) = 0. \tag{6}$$

Here $\hat{\tau}^*(\alpha) \equiv \varphi_\alpha^*(\alpha)/|\varphi_\alpha^*(\alpha)|$ is a unit tangent vector to the string, $\lambda(\alpha)$ is a Lagrange multiplier that imposes the constraint (3) or (4), and $[\nabla V]^{\perp} = \nabla V - (\nabla V \cdot \hat{\tau})\hat{\tau}$.

A simple way of finding a string that satisfies Eq. (6) is by steepest-descent dynamics in string space,[4]

$$\dot{\varphi}(\alpha;t) = -\{\nabla V[\varphi(\alpha;t)]\}^{\perp} + \lambda(\alpha;t)\hat{\tau}(\alpha;t). \tag{7}$$

Here the time t labels the string configurations during steepest descent and $\dot{\varphi} = \partial\varphi/\partial t$. We notice that within the nudged elastic band method[3] the search for a MEP is based on the equation

$$\dot{\varphi}(\alpha;t) = -\{\nabla V[\varphi(\alpha;t)]\}^{\perp} + k\left\{\frac{\partial^2\varphi(\alpha;t)}{\partial\alpha^2}\hat{\tau}(\alpha;t)\right\}\hat{\tau}(\alpha;t), \tag{8}$$

where k is an adjustable parameter, representing the elastic constant of the string, i.e., the elastic band in this context. We see that in Eq. (8) the Lagrange multiplier $\lambda(\alpha,t)$ of Eq. (7) is replaced by a penalty function; otherwise the two approaches are equivalent.

In this paper we follow the string method, but rather than using Eq. (7) we use second-order damped molecular dynamics to find a MEP: the advantage of this approach over steepest-descent dynamics has been discussed in Ref. 12. The damped molecular dynamics equation is

$$\ddot{\varphi}(\alpha;t) = -\{\nabla V[\varphi(\alpha;t)]\}^{\perp} - \gamma_s\dot{\varphi}(\alpha;t) + \lambda(\alpha;t)\hat{\tau}(\alpha;t). \tag{9}$$

Here γ_s is a friction coefficient that we use as an adjustable parameter to speed up the convergence. Equation (9) is integrated numerically by a simple modification of the Verlet algorithm that includes the friction term

$$\varphi(\alpha;t+\Delta) = \frac{f_s-1}{f_s+1}\varphi(\alpha;t-\Delta) + \frac{2}{f_s+1}\varphi(\alpha;t) + \frac{\Delta^2}{f_s+1}F(\alpha;t). \tag{10}$$

Here Δ is the time step, $F = -[\nabla V]^{\perp} + \lambda\hat{\tau}$ is the force due to the potential and the constraint, $f_s = \gamma_s\Delta/2$ is an effective friction parameter having a value between 0 and 1. The value $f_s = 0$ corresponds to conservative dynamics (no damping), while the value $f_s = 1$ corresponds to steepest-descent dynamics (overdamping). Numerically, we adopt a discrete representation of a string, in which the continuous parameter α is replaced by an integer $l = 0,1,2,...,P$. In this way a string becomes a chain of $P+1$ replicas, obeying equation

$$\varphi(l;t+\Delta) = \frac{f_s-1}{f_s+1}\varphi(l;t-\Delta) + \frac{2}{f_s+1}\varphi(l;t) + \frac{\Delta^2}{f_s+1}F(l;t). \tag{11}$$

In order to calculate the force $F(l;t)$ in Eq. (11) we need to specify how the unit tangent vector $\hat{\tau}(l;t)$ and the Lagrange multiplier $\lambda(l;t)$ are calculated. This is discussed in Appendixes A and B, respectively.

B. First-principles string molecular dynamics

In FPMD (Refs. 2 and 15) the atomic PES is derived "on the fly" from the instantaneous ground state of the electrons. The latter is described within DFT. In FPMD the atomic coordinates $\{R\}$ and the single-particle Kohn–Sham (KS) orbitals of DFT $\{\psi\}$ are updated simultaneously according to the Car–Parrinello (CP) equations

$$\begin{aligned} M_I\ddot{R}_I &= -\frac{\partial E[\{R\},\{\psi\}]}{\partial R_I}, \\ \mu\ddot{\psi}_n &= -\frac{\delta E[\{R\},\{\psi\}]}{\delta\psi_n^*} + \sum_m \Lambda_{nm}\psi_m. \end{aligned} \tag{12}$$

Here $E[\{R\},\{\psi\}]$ is the DFT energy functional, M_I are the atomic masses, μ is a fictitious "mass" of the KS orbitals, for which we adopt the preconditioning scheme of Ref. 12, and Λ_{nm} are Lagrange multipliers that enforce orthogonality of the KS orbitals. With an appropriate choice of the electronic mass parameter and of the initial condition, the electrons follow adiabatically the atomic motion and Eq. (12) reproduces closely Born–Oppenheimer's atomic dynamics. To find local minima on the PES, friction terms are inserted in Eq. (12), i.e.,

$$\begin{aligned} M\ddot{R}_I &= -\frac{\partial E[\{R\},\{\psi\}]}{\partial R_I} - \gamma_a M\dot{R}_I, \\ \mu\ddot{\psi}_n &= -\frac{\delta E[\{R\},\{\psi\}]}{\delta\psi_n^*} - \gamma_e\mu\dot{\psi}_n + \sum_m \Lambda_{nm}\psi_m. \end{aligned} \tag{13}$$

Here we have eliminated the subscript I on the atomic mass M, because for the purpose of minimization it is convenient to assign the same mass to all the atoms. Typically, we take an average atomic mass value for M and adjust the relative speed of electronic and atomic dynamics with our choice of μ, but the true independent parameter is the ratio μ/M. The atomic (γ_a) and electronic (γ_e) friction coefficients are adjustable parameters to speed up convergence. Since the damped MD equations (13) are coupled, the two friction coefficients are not independent. Usually a good choice is to take a very small, or even zero, atomic friction and use the electronic friction as a parameter to control the efficiency of the local minimization.

In order to extend the CP approach to string dynamics, we associate KS orbitals $\{\psi^\alpha\}$ to all the atomic configurations $\{R^\alpha\}$ in a string. The equivalent of Eq. (13) for a string are

$$\begin{aligned} M\ddot{R}_I^\alpha &= -\left[\frac{\partial E[\{R^\alpha\},\{\psi^\alpha\}]}{\partial R_I^\alpha}\right]^{\perp} - \gamma_a M\dot{R}_I^\alpha + \lambda(\alpha)\hat{\tau}_I(\alpha), \\ \mu\ddot{\psi}_n^\alpha &= -\frac{\delta E[\{R^\alpha\},\{\psi^\alpha\}]}{\delta(\psi_n^\alpha)^*} - \gamma_e\mu\dot{\psi}_n^\alpha + \sum_m \Lambda_{nm}^\alpha\psi_m^\alpha. \end{aligned} \tag{14}$$

Here the superscript $\perp$ indicates the components of a vector orthogonal to the string. The first equation in Eq. (14) is just Eq. (9) where we have included an atomic mass M to facilitate comparison with Eq. (13). The same choice of parameters $(M,\mu,\gamma_a,\gamma_e)$ that works in Eq. (13) can be used in Eq. (14), with the identification $\gamma_s=\gamma_a$.

In numerical applications, the continuous parameter α is replaced by an integer $I=0,1,...,P$, as discussed in the preceding section, and we use a modified Verlet algorithm, like in Eq. (11), to integrate the damped MD equations for the string and the KS orbitals. The same algorithm can be used in Eq. (13) to find a local minimum on the PES. In this case several hundred iterations are usually sufficient to find a local minimum with good accuracy. A similar number of iterations are sufficient to find a MEP with Eq. (14). Therefore the numerical cost of string minimization is roughly equivalent to the cost of structural optimization by damped MD times a factor $P-1$, which is the number of replicas that are optimized with Eq. (14).

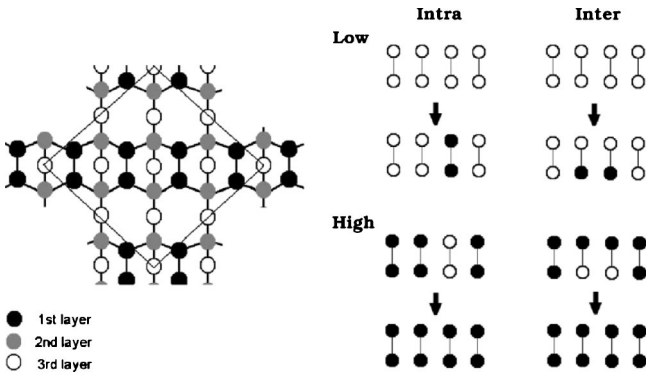

FIG. 1. Left: Schematic top view of the reconstructed Si(100) surface. The $p(\sqrt{8}\times\sqrt{8})$ R45° cell used for the calculations is indicated by the square. Right: Schematic representation of the four investigated processes: *intradimer* and *interdimer* pathways for H_2 adsorption on Si(100) surface at low and high H coverages. In each case, the initial and final states of the surface are shown. Empty and filled circles represent Si atom site and H-adsorbed Si atom site, respectively.

III. APPLICATION: H_2 ADSORPTION ON SI(100)

In this section we test our FPSMD implementation by studying a surface chemical reaction for which numerous experimental and theoretical results are available, namely, the adsorption of H_2 on the dimer-reconstructed Si(100) surface. This reaction has been intensively investigated for many years, both because of its technological importance and as a model for a more general understanding of chemisorption on covalent surfaces.[16–18] For a long time, the so-called *intradimer* pathway for H_2 dissociative adsorption on a single Si surface dimer has been widely accepted, but several controversial issues remained. In fact, more recent experiments have shown that an *interdimer* mechanism is actually operative. Evidence for such a pathway has been initially provided for the case of a partially hydrogenated Si(100) surface,[19,20] but somewhat later the interdimer mechanism has been found to be preferred also on the clean surface.[21] These experimental results have been further supported by theory. DFT calculations by Pehlke[22] found adsorption barriers of 0.35, 0.20, and 0.0 eV for the H2* (intradimer), H2 (interdimer on the clean surface), and H4 (interdimer on partially hydrogenated dimers) mechanisms, respectively, without inclusion of zero-point energies (ZPE). Similar trends have been also obtained in a very recent quantum Monte Carlo study:[23] Using cluster models of increasing sizes, and TS geometries determined at the DFT level, adsorption barriers of 0.75 ± 0.05, 0.63 ± 0.09, and 0.19 ± 0.14 eV (the first two inclusive of a ZPE contribution of 0.09 eV) were extrapolated for the H2*, H2, and H4 mechanisms, respectively. In the following the string method is applied to study H_2 adsorption on both the clean and partially hydrogenated Si(100) surfaces (see Fig. 1).

Computational details. Calculations have been performed using the Perdew–Burke–Ernzerhof exchange-correlation functional,[24] ultrasoft[25,26] and Troullier–Martins[27] pseudopotentials for H and Si, respectively, a plane-wave kinetic energy cutoff $E_{cut}=20$ Ry, a smooth charge density cutoff of 80 Ry, and an augmented charge density cutoff of 160 Ry. With these choices, we determined a H_2 bond length of 0.75 Å (experimental value of 0.74 Å) and an equilibrium lattice constant for bulk Si of 5.475 Å (experimental value of 5.43 Å). Such a slight overestimate of the lattice parameters is very frequent when using gradient corrected functionals.

The clean reconstructed Si(100) surface shows rows of buckled Si dimers with alternating buckling directions, resulting in a $c(4\times2)$ ground state periodicity. To model this surface, we used a slab of six Si layers and a surface $p(\sqrt{8}\times\sqrt{8})$ R45° supercell with eight atoms/layer (Fig. 1). Although this supercell does not accommodate the $c(4\times2)$ periodicity, but rather a $p(2\times2)$ one, the very small difference in energy between the $p(2\times2)$ and the $c(4\times2)$ structures is known to be irrelevant for the focus of this work.[22] The bottom two layers of the slab were held fixed at the bulk positions and the lower surface was terminated with H atoms. Electronic states at the Γ point only were used to represent the electronic charge density. With these settings, the buckling angle of the dimers on the clean surface was found to be about 18°.

For the calculation of the MEP by the string method, as the initial state we took a configuration with H_2 placed 4.23 Å above the surface, so that their interaction is practically negligible. For the replicas, the starting configurations were constructed by linear interpolation between the initial and final states. Ten replicas were used to represent the string, which was optimized until the residual force $-\nabla V^{\perp}$ was less than 0.05 eV/Å for all movable ions. Because we use a discrete string representation, a TS does not usually coincide with the configuration of any replica on the string. Starting from a replica adjacent to the TS we can, however, easily locate the TS exactly within numerical accuracy. This can be achieved by relaxing the replica uphill, in the direction of the string, and downhill, in the hyperplane orthogonal to the string. This technique was used to locate the exact saddle point with the forces being less than 0.05 eV/Å for all mobile ions. For the interdimer path at high coverage, an additional string calculation with four replicas was performed to gain a

TABLE I. Reaction energies (E_{rxn}) and barriers ($E^{\ddagger}_{ads}$), in eV, for H_2 adsorption on Si(100) through intradimer and interdimer pathways at low and high H coverages. Intra (low), Inter (low), and Inter (high) correspond to H2*, H2, and H4, respectively, in Ref. 22.

	E_{rxn}		$E^{\ddagger}_{ads}$	
	This work	Reference[a]	This work	Reference[b]
Intra (low)	1.94	1.95	0.40	0.37
Intra (high)	2.03	2.06	0.45	
Inter (low)	1.67	1.64	0.24	0.20
Inter (high)	2.41	2.41	0.0	0.0

[a]Reference 22.
[b]Reference 23.

higher resolution in a portion of the path where a steep change in energy was observed (Fig. 5).

Results. Reaction energies (E_{rxn}) are summarized in Table I. For the clean surface, the H_2 adsorption energy for the intradimer configuration is higher than the interdimer adsorption energy by ≈0.3 eV, while the reverse is true for the high coverage limit. These differences can be understood in terms of H-pairing effects, which favor configurations where both dangling bonds of a Si dimer are saturated by H atoms.[28] The computed increase in adsorption energy for increasing H coverage is consistent with experiments[29] and with previous DFT calculations.[22]

The potential energy profiles along the intradimer and interdimer MEPs at low H coverage are shown in Fig. 2, and the geometrical parameters for the corresponding transition states are summarized in Table II. It appears that the interdimer barrier is lower than the intradimer one (see also Table I), in agreement with recent calculations.[22,23] The geometry of the intradimer TS is also very similar to that found in previous calculations.[30,31] Structures close to the TS are shown for both MEPs in Figs. 3 and 4.

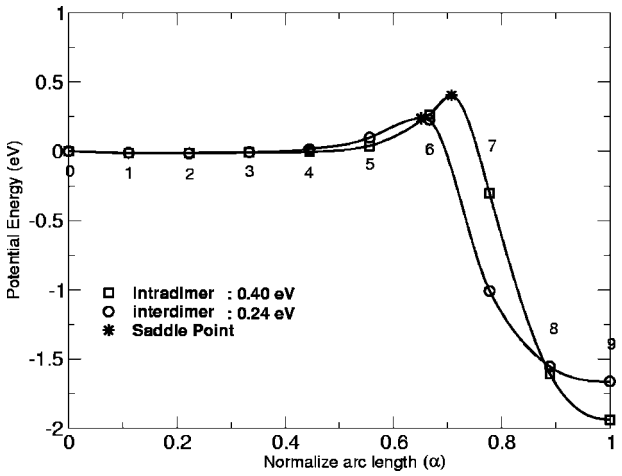

FIG. 2. Potential energy profile along the MEP for H_2 adsorption on Si(100) at low H coverage. The energy zero corresponds to the potential energy of the noninteracting H_2 molecule and Si(100) surface. Ten replicas are used to represent the string. The location of the saddle point (exact TS) is indicated by the star. A cubic polynomial was used for interpolation between adjacent replicas. The interdimer and the intradimer pathways have barriers of 0.24 and 0.40 eV, respectively.

TABLE II. Structural parameters of the Intra (low) and Inter (low) transition states. Bond lengths are in angstroms, and buckling angle in degree. See Figs. 3 and 4 for atom indices.

	Intra	Inter
H1-H2 (Å)	1.00	0.91
H1-Si1 (Å)	1.69	1.98
H2-Si1 (Å)	1.77	1.97
Si1-Si2 (Å)	2.46	3.61
Angle (deg)	13.8	

To analyze the changes of the chemical bonds in the reaction, it is useful to examine the maximally localized Wannier functions[32,33] (MLWFs) of replicas close to the TS along the various pathways. MLWFs are unitary transformations of the molecular orbitals such that the resulting orbitals are maximally localized in space. These localized orbitals are closely associated to the chemical ''bonds'' in the system. In the intradimer pathway, the H_2 molecule does not approach the surface directly above the center of the Si dimers, but is shifted toward the lower Si atom. Thus the lower empty Si dangling bond (DB) accepts electrons from the H_2 molecule (Fig. 3). Similarly, in the interdimer pathway, the H_2 molecule slightly shifts towards the dimer with the lower Si atom where the DB is empty (Fig. 4). We observe an increasing delocalization of the MLWFs corresponding to the intramolecular H_2 bond as the transition takes place. Also the electronic state localized on the upper Si atom becomes noticeably more delocalized close to the TS, suggesting a concomitant reduction of the HOMO-LUMO gap, where HOMO and LUMO stands for highest occupied and lowest unoccupied molecular orbitals.[34]

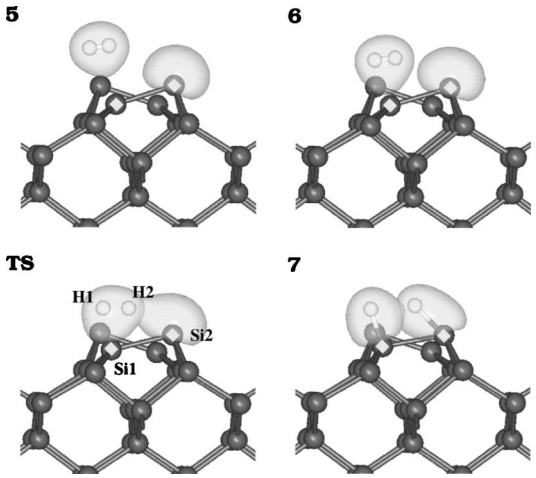

FIG. 3. MEP for H_2 intradimer adsorption at low H coverage: a few replicas around the TS are shown. Gray and white atoms are Si and H atoms, respectively. The replica index is indicated at the upper left corner. The Si atoms on which the H_2 adsorbs are marked by a diamond shape, and the view direction is $[1\bar{1}0]$. Isosurfaces (at 0.01 a.u.) of the electron density are shown for the two relevant MLWFs involved in the transition. In our spin-restricted calculations, a single MLWF represents two electrons. One MLWF is initially localized on the H_2 molecule, and the other on the buckled Si dimer. A substantial overlap of the electron density at the transition state is evident.

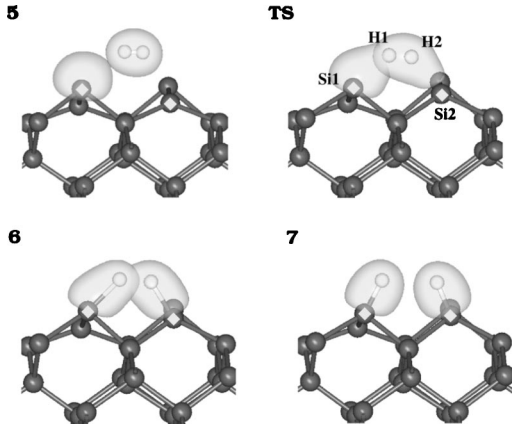

FIG. 4. MEP for H_2 interdimer adsorption at low H coverage: A few replicas around the TS are shown. The Si atoms on which the H_2 adsorbs are marked by a diamond shape, and the view direction is [110], i.e., rotated by 90° with respect to Fig. 3. Isosurfaces (at 0.01 a.u.) of the electron density are shown for the two relevant MLWFs involved in the transition. One MLWF is initially localized on the H_2 molecule, and the other on the buckled Si dimer whose "up" atom is close to the H_2 molecule. Other details are same as in Fig. 3.

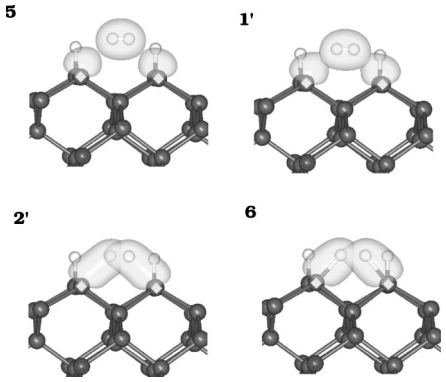

FIG. 6. Details of the interdimer MEP at high H coverage. Replicas 1′ and 2′ are obtained from an additional string calculation between replicas 5 and 6 of Fig. 5. The Si atoms on which the H_2 adsorb are marked by a diamond shape, and the view direction is [110]. Isosurfaces (at 0.01 a.u.) of the electron density are shown for two relevant MLWFs involved in the transition. One MLWF results from the electrons initially belonging to H_2. Another MLWF exhibits a higher density at two ends of different Si dimers, representing two dangling bonds situated on different Si dimers. A substantial rearrangement of chemical bonds, occurring around replicas 1′ and 2′, yields the steep change in the potential energy profile observed in Fig. 5. Other details are same as in Fig. 3.

At high coverage, the MEP for the interdimer pathway shows no potential energy barrier (Fig. 5), which is in accordance with previous results.[20,22] The barrier for the intradimer pathway, 0.45 eV, is slightly higher than in the low coverage limit, which can be related to the fact that the hydrogenated surface tends to be more "rigid" than the clean one. However, it is clear that the intradimer pathway is not affected as much as the interdimer one by the presence of other H atoms on the surface. The significant change in the nature of interdimer MEP from the low to high H-coverage limit can be understood considering the high reactivity of the partially occupied Si dimers which have one unpaired DB electron at energy well above all other occupied states.[20] The drastic gradient change observed in the potential energy profile along the interdimer MEP (around replicas indexed with 1′ and 2′) is the result of the strong rearrangement of the electronic structure when the H-Si bonds are formed (Fig. 6).

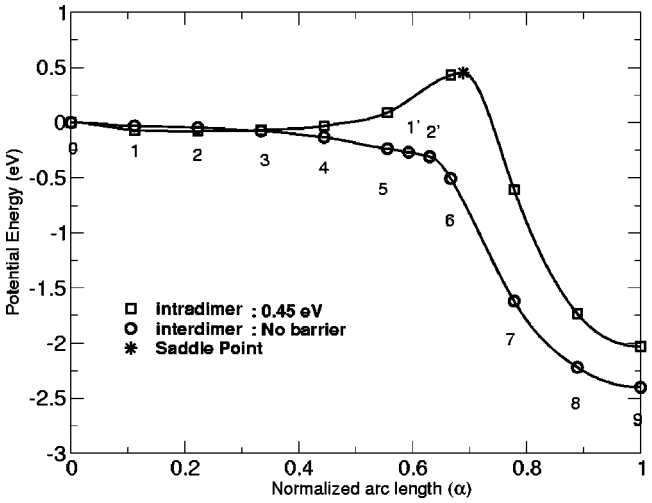

FIG. 5. Potential energy profile along the MEP for H_2 adsorption on the Si(100) surface at high H coverage. The energy zero corresponds to the potential energy of the noninteracting H_2 molecule and H/Si(100) surface. Ten replicas were used to represent the string. No potential energy barrier was found for the interdimer path, and an additional string calculation (points 1′ and 2′) was carried out between replicas 5 and 6 for a better resolution around that region. Other details are same as in Fig. 2.

Thus, in agreement with previous results,[20–22] our calculations indicate that the interdimer path is likely to be operative at both low and high H coverages on the Si(100) surface. The discrepancy between the low-coverage interdimer adsorption energy barrier of 0.24 eV, predicted by our calculations as well as by Ref. 22, and the experimental value of 0.6–0.7 eV (Ref. 20) is most probably a shortcoming of the adopted DFT approximations, as suggested by the quantum Monte Carlo results of Ref. 23.

Efficiency of the string method for $H_2/Si(100)$. As stated earlier, the effort (i.e., CPU time) involved in a string calculation is very close to that of relaxing $P-1$ different configurations of the system, where $P-1$ is the number of "mobile" replicas in the string. For each of the pathways mentioned above, between several hundred and a thousand steps of combined ionic and electronic damped dynamics were necessary to optimize the replicas representing the string. Once the MEP was obtained from a string calculation, identification of the TS was quite straighforward.

The dependence of the MEP on the initial state of the reaction was tested for the intradimer pathway in the low-coverage limit by performing calculations for a few different orientations and positions of the H_2 molecule above the surface. The string always converged to the same MEP, at least in the region near the TS, even if the number of steps could somewhat vary, e.g., between a 1000 and 1500. This result also indicates that the PES for $H_2/Si(100)$ is quite smooth, which is the situation in which the string method, especially in our current implementation, can be effectively applied. In

the same context, we notice that in our calculations the (low-coverage) interdimer MEP was obtained by taking two H atoms on adjacent dimers as final state of the reaction. For two H atoms on the otherwise clean surface, however, the true ground state corresponds to both hydrogens on the same dimer. Finding the interdimer pathway when such a ground state is taken as the final state of the reaction is in principle possible, but in practice very unlikely. In other words, we cannot expect the string method to work so efficiently that no ''chemical intuition'' of the system under study would be necessary.

Most of the early studies of $H_2/Si(100)$ were based on an extensive sampling of the PES, in which the total energy was first calculated for a large number (a hundred or more) of configurations, characterized by assigned values of a few ''reaction parameters.'' After approximate location of the TS, a finer sampling, typically requiring many further evaluations of the total energy, was carried out. Even as a local optimization procedure restricted to a smooth PES, our current implementation of the string method is substantially more efficient than performing such an extensive sampling of the PES, with the additional advantage of a simpler and more accurate identification of the TS. The relative efficiency of our approach with respect to the NEB method was not tested, but given the similarity of the two methods, we expect that also their efficiency should be similar when an appropriate value for the NEB elastic constant [k in Eq. (8)] is used.

IV. CONCLUSIONS

We have presented an efficient implementation of the string method within FPMD. Using the example of the adsorption of H_2 on the Si(100) surface, we have demonstrated the effectiveness of FPSMD in finding MEPs on a potential energy surface of DFT quality. In addition to locating TS, the MEP is also useful to qualitatively understand chemical reaction mechanisms. In particular, the chemical bond rearrangements that take place in a reaction can be monitored nicely by studying the evolution of the MLWFs along a MEP.

As is generally the case with approaches based on a ''chain of states'' method, FPSMD is amenable to efficient parallelization. This follows from the fact that the computationally expensive part of the calculation, i.e., the evaluation of the gradient of the PES, is done independently for each replica. Coupling between the replicas appears only in the computation of the constraint force, a procedure that requires negligible memory and CPU time. Thus, if the number of replicas needed to represent a reaction path is not exceedingly large, we should expect that relatively large systems consisting of up to few hundred atoms could be studied with FPSMD using modern parallel computational platforms.

The FPSMD formulation that we have presented applies to zero temperature, i.e., when the PES is the most important factor in determining a reaction pathway and entropic effects can be neglected. An advantage of the string over the NEB method is that it can be extended rather directly to finite temperature. We will discuss in a future paper a convenient finite temperature formulation of FPSMD. This will allow us to deal with more general reaction events and compute free energy rather than potential energy barriers.

Several important issues remain open to future investigation. One concerns the relation between MEPs and chemical reaction rates. So far we have implicitly assumed that rates can be calculated from TST. More accurate calculations including dynamical corrections[35,36] to TST are beyond our present scope. Even in this more general context, however, the information provided by string method at zero and finite temperature should be a useful input for more accurate dynamical rate calculations.

Another relevant issue concerns the accuracy of current DFT approximations to compute energy (and free energy) barriers. It is still premature to make general statements on the DFT accuracy for reaction barriers, because highly accurate experimental and/or theoretical data on barrier heights are currently limited. There are examples, however, like the Si(100) hydrogenation reactions discussed in this paper, where generalized gradient approximations (GGA) of DFT appear to yield barrier heights that are underestimated compared to experiment or to more accurate theoretical approaches. More quantitative barrier determinations may require more accurate DFT functionals. For example, hybrid DFT functionals agree quite well with the quantum Monte Carlo results in Ref. 23. When considering the hydrogenation of the Si(100) surface, however, GGA gives correctly the qualitative aspects of the reaction as well as the trends at varying experimental conditions. Thus, in spite of some limitations, we expect that FPSMD can provide, for a large class of systems, crucial details of the reaction mechanisms and help understand the important experimental observations.

ACKNOWLEDGMENTS

We thank W. E for introducing us to the string method. We also thank W. Ren, V. Srinivasan, and N. Takeuchi for helpful discussions, and M. Sharma for making his code available for calculations of the MLWFs. This work was partially supported by NSF Award No. CHE-0121432. Calculations were performed at the W. M. Keck Computational Materials Science Computing Center of PRISM.

APPENDIX A: UNIT TANGENT VECTOR

Equation (11) requires knowledge of the unit tangent vectors $\hat{\tau}(l)$ at all $P+1$ points in a discrete string representation. In a continuous string the unit tangent vector is $\hat{\tau}(\alpha) \equiv \varphi_\alpha(\alpha)/|\varphi_\alpha(\alpha)|$. The discrete version of this formula requires $\varphi_\alpha(l)$, i.e., the derivative of a curve $\varphi(\alpha)$ at the $P+1$ points of its discrete representation. For this we adopt a prescription given by Henkelman and Jónsson[8] who define the derivative vector $\varphi_\alpha(l)$ as follows. If the PES behaves monotonically at l the derivative is defined as

$$\varphi_\alpha(l) \equiv \begin{cases} \varphi_\alpha^+(l) = \dfrac{1}{\Delta\alpha}[\varphi(l+1)-\varphi(l)] & \text{if } V(l+1)>V(l)>V(l-1) \\ \varphi_\alpha^-(l) = \dfrac{1}{\Delta\alpha}[\varphi(l)-\varphi(l-1)] & \text{if } V(l+1)<V(l)<V(l-1). \end{cases} \tag{A1}$$

Here $\Delta\alpha = 1/P$ is the spacing between adjacent points on a discrete string. If the potential has a maximum or a minimum at l the derivative is defined as a weighted average of φ_α^+ and φ_α^-,

$$\varphi_\alpha(l) \equiv \begin{cases} a\varphi_\alpha^+(l) + b\varphi_\alpha^-(l) & \text{if } V(l+1)>V(l-1) \\ b\varphi_\alpha^+(l) + a\varphi_\alpha^-(l) & \text{if } V(l+1)<V(l-1). \end{cases} \tag{A2}$$

The weights a and b are given by

$$a = \frac{\Delta V_{\max}(l)}{\Delta V_{\max}(l) + \Delta V_{\min}(l)}, \qquad b = \frac{\Delta V_{\min}(l)}{\Delta V_{\max}(l) + \Delta V_{\min}(l)}. \tag{A3}$$

Here $\Delta V_{\max}(l) = \max(|V(l+1)-V(l)|, |V(l-1)-V(l)|)$ and $\Delta V_{\min}(l) = \min(|V(l+1)-V(l)|, |V(l-1)-V(l)|)$. Finally, the unit tangent vector $\hat{\tau}(l)$ is obtained by normalizing the derivative vector $\varphi_\alpha(l)$.

APPENDIX B: LAGRANGE MULTIPLIER

Equation (9), i.e., our equation for string dynamics, contains a Lagrange multiplier $\lambda(\alpha;t)$. This is uniquely specified by the constraint Eq. (4) and the equation of motion, and can be calculated analytically. If the initial state of a string satisfies the constraint, the analytic expression for the Lagrange multiplier ensures that the constraint will be exactly satisfied at all subsequent times in the dynamical evolution. This procedure, however, is not appropriate in numerical simulations because the latter are based on an approximate solution of the equation of motion using a finite difference formula like Eq. (11). In this case, use of the exact analytic expression for $\lambda(\alpha;t)$ would lead to increasingly large errors in the constraint as the approximate dynamics evolves from an initial state that satisfies the constraint. The correct approach to follow in numerical simulations was pointed out by Ryckaert *et al.*[14] It consists in finding, at each time step, a new Lagrange multiplier that enforces the constraint with accuracy consistent with that of the numerical integrator. This is the procedure we adopt here.

A string is updated using Eq. (11), i.e.,

$$\varphi(l;t+\Delta) = \frac{f_s-1}{f_s+1}\varphi(l;t-\Delta) + \frac{2}{f_s+1}\varphi(l;t) + \frac{\Delta^2}{f_s+1}\{-[\nabla V(l;t)]^\perp + \lambda(l;t)\hat{\tau}(l;t)\}. \tag{B1}$$

This equation can be written as

$$\varphi(l;t+\Delta) = \overline{\varphi}(l;t+\Delta) + x(l;t)\hat{\tau}(l;t). \tag{B2}$$

Here, $\overline{\varphi}(l;t+\Delta) \equiv (f_s-1)/(f_s+1)\varphi(l;t-\Delta) + 2/(f_s+1)\varphi(l;t) + \Delta^2/(f_s+1)(-[\nabla V(l;t)]^\perp)$ is the predicted string at time $t+\Delta$ without taking the constraint into account, and $x(l;t) \equiv \Delta^2/(f_s+1)\lambda(l;t)$ is the unknown Lagrange multiplier to be determined by the condition (4) at time $t+\Delta$. This condition requires the derivative vector $\varphi_\alpha(l)$, which should be evaluated, in principle, using the formulas of Appendix A. In practice, to impose the constraint it is sufficient to approximate $\varphi_\alpha(l)$ with either $\varphi_\alpha^+(l)$ or $\varphi_\alpha^-(l)$ in Eq. (A1), independently of whether the potential is monotonic or has a local maximum or minimum at l. In what follows we take

$$\varphi_\alpha(l) = \varphi_\alpha^+(l) = P[\varphi(l+1)-\varphi(l)]. \tag{B3}$$

Then, for a discrete string, Eqs. (4) and (5) become

$$|\varphi(l+1)-\varphi(l)|^2 = c, \tag{B4}$$

and

$$\sum_{l=0}^{P-1} |\varphi(l+1)-\varphi(l)|^2 = cP, \tag{B5}$$

respectively. Here a factor $1/P^2$ has been included in the constant c.

Equation (B4) should be satisfied for all values of l between 0 and $P-1$. Given condition (B5), there are $P-1$ independent equations of the form (B4). These are sufficient to determine uniquely the $P-1$ unknown Lagrange multipliers $x(l)$ for $1 \leqslant l \leqslant P-1$. Notice that $x(0) = x(P) = 0$ because the end points of a string are held fixed. By imposing Eq. (B4) at time $t+\Delta$ and using Eq. (B2), we get

$$|\overline{\varphi}(l+1;t+\Delta) - \overline{\varphi}(l;t+\Delta) + x(l+1;t)\hat{\tau}(l+1;t) - x(l;t)\hat{\tau}(l;t)|^2 = c. \tag{B6}$$

In what follows we omit the time dependence in Eq. (B6) and define $\Delta\overline{\varphi}(l) \equiv \overline{\varphi}(l+1) - \overline{\varphi}(l)$. Given the accuracy of the numerical integrator, Eq. (B2), it is sufficient to satisfy the constraint to $O(\Delta^4)$. Recalling that $x(l)$ is $O(\Delta^2)$, this means that the dependence on $x(l)$ and $x(l+1)$ in Eq. (B6) can be linearized, i.e.,

$$|\Delta\overline{\varphi}(l)|^2 + 2[x(l+1)\hat{\tau}(l+1) - x(l)\hat{\tau}(l)]\cdot\Delta\overline{\varphi}(l) = c. \tag{B7}$$

Equation (B7) allows us to express $x(l+1)$ in terms of $x(l)$

$$x(l+1) = \frac{c - |\Delta\overline{\varphi}(l)|^2 + 2x(l)\hat{\tau}(l)\cdot\Delta\overline{\varphi}(l)}{2\hat{\tau}(l+1)\cdot\Delta\overline{\varphi}(l)}. \tag{B8}$$

Since $x(0) = 0$, Eq. (B8) would provide the Lagrange multipliers if we knew the constant c. This constant could be determined by the condition $x(P) = 0$ or by Eq. (B5). For numerical purposes, however, it is more convenient to deter-

mine the constant c with a self-consistent iterative procedure, starting with an estimate from the previous time step. We call this initial estimate $c^{(0)}$; inserting it in Eq. (B8) we obtain an estimate $x^{(0)}(l)$ for the Lagrange multipliers; inserting $x^{(0)}(l)$ in Eq. (B2) we obtain an estimate $\varphi^{(0)}(l)$ for the string at time $t+\Delta$; this in turn is used to obtain a better estimate for the constant c from Eq. (B5); we call this estimate $c^{(1)}$ and iterate the entire procedure, and so on and so forth. A few iterations are sufficient to get highly accurate values for both c and the Lagrange multipliers $x(l)$. The computational cost associated with the iterative calculation of the constraint force is negligible when compared to the cost of calculating the gradient of the PES within first-principles DFT.

[1] D. Chandler, in *Classical and Quantum Dynamics in Condensed Phase Simulations*, edited by B. J. Berne, G. Ciccoti, and D. F. Coker (World Scientific, Singapore, 1998), and references therein.
[2] R. Car and M. Parrinello, Phys. Rev. Lett. **55**, 2471 (1985).
[3] H. Jónsson, G. Mills, and K. Jacobson, in *Classical and Quantum Dynamics in Condensed Phase Simulations*, edited by B. J. Berne, G. Ciccoti, and D. F. Coker (World Scientific, Singapore, 1998).
[4] W. E, W. Ren, and E. Vanden-Eijnden, Phys. Rev. B **66**, 052301 (2002).
[5] J. VandeVondele and U. Rothlisberger, J. Am. Chem. Soc. **124**, 8163 (2002).
[6] H. Eyring, J. Chem. Phys. **3**, 107 (1934).
[7] See, e.g., F. Jensen, *Introduction to Computational Chemistry* (Wiley, New York, 1999).
[8] G. Henkelman and H. Jónsson, J. Chem. Phys. **113**, 9978 (2000).
[9] G. Henkelman and H. Jónsson, Phys. Rev. Lett. **86**, 664 (2001).
[10] J. Greeley and M. Mavrikakis, J. Am. Chem. Soc. **124**, 7193 (2001).
[11] I. M. Chiobica, F. Freschardi, R. A. van Santen, A. W. Kleyn, and J. Hafner, J. Phys. Chem. B **104**, 3364 (2000).
[12] F. Tassone, F. Mauri, and R. Car, Phys. Rev. B **50**, 10561 (1994).
[13] D. Marx and M. Parrinello, J. Chem. Phys. **104**, 4077 (1996).
[14] J. Ryckaert, G. Ciccotti, and H. J. C. Berendsen, J. Comput. Phys. **23**, 327 (1977).
[15] For a recent review of the FPMD method, see, e.g., D. Marx and J. Hutter, in *Modern Methods and Algorithms of Quantum Chemistry*, edited by J. Grotendorst (NIC, FZ Jülich, 2000).
[16] J. M. Buriak, Chem. Rev. (Washington, D.C.) **102**, 1272 (2002).
[17] R. A. Wolkow, Annu. Rev. Phys. Chem. **50**, 413 (1999).
[18] S. F. Bent, Surf. Sci. **500**, 879 (2002).
[19] A. Biedermann, E. Knoesel, Z. Hu, and T. Heinz, Phys. Rev. Lett. **83**, 1810 (1999).
[20] M. Dürr, M. Raschke, E. Pehlke, and U. Höfer, Phys. Rev. Lett. **86**, 123 (2001).
[21] M. Dürr, Z. Hu, A. Biedermann, U. Höfer, and T. Heinz, Phys. Rev. Lett. **88**, 046104 (2002).
[22] E. Pehlke, Phys. Rev. B **62**, 12932 (2000).
[23] C. Filippi, S. B. Healy, P. Kratzer, E. Pehlke, and M. Scheffler, Phys. Rev. Lett. **89**, 166102 (2002).
[24] J. Perdew, K. Burke, and M. Ernzerhof, Phys. Rev. Lett. **77**, 3865 (1996).
[25] D. Vanderbilt, Phys. Rev. B **41**, 7892 (1990).
[26] K. Laasonen, R. Car, C. Lee, and D. Vanderbilt, Phys. Rev. B **43**, 6796 (1991).
[27] N. Troullier and J. Martins, Phys. Rev. B **43**, 1993 (1991).
[28] A. Vittadini, A. Selloni, and M. Casarin, Phys. Rev. B **49**, 11191 (1994).
[29] M. Raschke and U. Höfer, Phys. Rev. B **63**, 201303 (2001).
[30] E. Penev, P. Kratzer, and M. Scheffler, J. Chem. Phys. **110**, 3986 (1999).
[31] J. Steckel, T. Phung, and K. Jordan, J. Phys. Chem. B **105**, 4031 (2001).
[32] N. Marzari and D. Vanderbilt, Phys. Rev. B **56**, 12847 (1997).
[33] M. Sharma, Y. Wu, and R. Car, Int. J. Quantum Chem. **95**, 821 (2003).
[34] R. Resta, J. Phys.: Condens. Matter **14**, 625 (2002).
[35] D. Chandler, J. Chem. Phys. **68**, 2959 (1978).
[36] J. A. Montgomery, Jr., D. Chandler, and B. J. Berne, J. Chem. Phys. **70**, 4056 (1979).